This is a repository copy of *Long-term performance of GFRP bars in concrete elements under sustained load and environmental actions*.

White Rose Research Online URL for this paper:
http://eprints.whiterose.ac.uk/132400/

Version: Accepted Version

Article:
Fergani, H., Di Benedetti, M. orcid.org/0000-0001-7870-1323, Oller, C.M. et al. (2 more authors) (2018) Long-term performance of GFRP bars in concrete elements under sustained load and environmental actions. Composite Structures, 190. pp. 20-31. ISSN 0263-8223

https://doi.org/10.1016/j.compstruct.2018.02.002

Reuse
This article is distributed under the terms of the Creative Commons Attribution-NonCommercial-NoDerivs (CC BY-NC-ND) licence. This licence only allows you to download this work and share it with others as long as you credit the authors, but you can't change the article in any way or use it commercially. More information and the full terms of the licence here: https://creativecommons.org/licenses/

Takedown
If you consider content in White Rose Research Online to be in breach of UK law, please notify us by emailing eprints@whiterose.ac.uk including the URL of the record and the reason for the withdrawal request.

eprints@whiterose.ac.uk
https://eprints.whiterose.ac.uk/

Long-term performance of GFRP bars in concrete elements under sustained load and environmental actions

Hamed Fergani[a,*], Matteo Di Benedetti[a], Cristina Miàs Oller[b], Cyril Lynsdale[a], Maurizio Guadagnini[a]

[a] Department of Civil and Structural Engineering, University of Sheffield, Sheffield, S1 3JD, UK
[b] Analysis and Advanced Materials for Structural Design (AMADE), University of Girona, Girona, Spain

Abstract

This paper presents an experimental study aimed at investigating the long-term tension stiffening and flexural behaviour of concrete elements reinforced with glass fibre reinforced polymer (GFRP) bars subjected to accelerated aging conditions. Six tension stiffening specimens and eight small-scale GFRP RC beams were exposed to different environments and sustained stress levels for 120 and 270 days, respectively. Subsequently, the specimens were tested to failure and their behaviour was compared to that of reference specimens. The test results revealed that stressed specimens conditioned in a wet environment experienced a reduction in tension stiffening response as a result of bond degradation and a reduced stress transfer from the bar to the surrounding concrete. The results also indicate that the accelerated aging conditions affected the overall flexural behaviour and led to higher deflections and larger crack widths. The long-term deformation of elements subjected to a stress level representing typical in-service conditions, however, always complied with the design limits suggested by current guidelines. Higher imposed loads (inducing maximum strain level in the reinforcement of about 5000με) led to both deflections and crack widths in excess of the values recommended at serviceability limit state. Finally, the response of the tested specimens is compared to that predicted according to *fib* Model Code 2010 and Eurocode 2 and it is shown that both models fail to capture adequately the long-term structural behaviour of stressed GFRP RC specimens conditioned in wet environment.

Keywords

A. Glass fibres

B. Debonding

D. Mechanical testing

Environmental action

* Corresponding Author. Email address: hamed.fergani@sheffield.ac.uk

1 Introduction

The use of fibre reinforced polymer (FRP) bars, and in particular glass FRP (GFRP), as reinforcement in concrete structures to address corrosion-related issues is receiving a great deal of attention and a significant growth in field applications has been recorded in the past few years [1-4]. Despite being recognised as durable reinforcement, however, the work conducted in the past three decades has focused mainly on the short-term behaviour of FRP RC elements [5-12], and very few studies have investigated their long-term structural performance [13-15]. The limited experimental research on this topic, which is often inconclusive, is inadequate to demonstrate the long-term potential benefits of this new class of reinforcement. Experience from field studies is also limited due to the relatively young age of existing field applications. Thus, understanding the long-term performance of FRP RC elements at both serviceability and ultimate limit states is key to enable an optimal and safe design of more sustainable structures and infrastructure. Current design procedures and guidelines for FRP RC elements rely heavily on the outcome of short-term studies [16-19], hence their validity in predicting long-term performance needs to be carefully assessed, especially in terms of service conditions, which often govern the design.

Researchers have suggested modifications to Branson's equation to account for the relative low stiffness of FRP reinforcement on the effective moment of inertia when calculating short-term deflections of FRP RC elements [7-10,17], or have proposed modifications on the basis of observations on the more fundamental tension stiffening behaviour [11,20-23]. These different approaches have been implemented in current design guidelines for FRP RC (e.g. [24-27]) but have been shown to overestimate tension stiffening and underestimate deflections [28,29]. In addition, there is very limited research examining long-term tension stiffening response [e.g. 30], and no studies have been reported on the combined effects of severe environmental exposure and loading conditions on the long-term tension stiffening and flexural behaviour of GFRP RC members.

Exposure to different chemical environments, moisture, elevated temperatures or temperature variations can all cause degradation of the resin-rich outer layer, thus affecting the bond between bar and concrete, and affect adversely the bond between fibres and resin in the reinforcing bars [31]. Exposure to ordinary temperature cycles can also lead to bond degradation due to the difference in thermal expansion between the bar and the concrete [32]. All of these environmental conditions would cause a reduction in tension stiffening and affect the performance of GFRP RC members in bending.

This paper presents part of a multi-scale experimental programme that is aimed to provide a better understanding of the durability of GFRP bars in concrete. Accelerated tests on small and medium-scale bare bar

specimens [31,33] were complemented by accelerated tests on GFRP RC tension ties and small scale beams to examine the long-term bond and flexural behaviour of GFRP RC members under service conditions. Two different levels of sustained stress were considered in this study: 1) a stress inducing a level of strain in the FRP bar equivalent to 3000 με to generate a state of stress in the concrete surrounding the bars that is typical of prescribed service conditions; 2) a stress level inducing a level of strain in the FRP bar equivalent to 5000με to initiate greater damage in the surrounding concrete and promote a higher degradation rate.

Test results presented in this paper are used to assess the performance of existing tension stiffening models and predict the flexural behaviour of GFRP RC members. The outcome of this study will provide important insights into the durability of FRP bars in concrete and inform the development of more reliable design equations to predict the long-term behaviour of FRP RC elements under service conditions, in terms of both deflections and crack width.

2 Experimental test programme

This study is part of an extensive experimental programme carried out at the University of Sheffield that aims to examine the durability of GFRP bars in concrete members [31, 33]. Typical environmental conditions known to accelerate the degradation processes of GFRP bars in concrete structures were examined in this study, along with the application of given levels of sustained stress. A maximum temperature of 60°C was chosen based on tests recommended in different standards and employed in previous research [25, 34-36]. This level of temperature was found to be high enough to accelerate the degradation of the mechanical properties of the bars, yet still below the glass transition temperature expected for typical pultruded GFRP reinforcement. The length of exposure was also chosen on the basis of previous research employing accelerated tests and it was found to be appropriate to enable the onset and stabilisation of the main degradation processes [35, 36]. Six tension stiffening specimens (TS) and eight simply supported small-scale GFRP RC beams (BM) were exposed to different environments and sustained stress levels and load tested to study their long-term performance. The specimens are designated according to the format XX.ttt.TT°C.E.SS, where *XX* denotes the specimen typology, *ttt*, *TT°C* and *E* are the exposure time, temperature and environment(a=air, W= tap water), respectively, while *SS* represents the loading condition. For example, TS.120.60°C.W.3k is a tension stiffening specimen, exposed to water at 60°C with a sustained load inducing 3000με in the reinforcement for 120 days.

Tension stiffening specimens were square in cross-section (100 x 100 mm) and 1100 mm long with an effective bond length, l_c, of 500 mm (**Fig. 1**). After casting, these specimens were cured in water at 20°C to minimise the effects of drying shrinkage on the tension stiffening behaviour.

All RC beams were 110 mm wide, 150 mm deep and 1200 mm long, with a clear span of 1000 mm (**Fig. 2**). The longitudinal reinforcement consisted of two ribbed GFRP bars in tension and two sand coated basalt FRP (BFRP) bars in compression (**Fig. 3**). The GFRP bars used in this research were made of continuous longitudinal glass fibres impregnated in vinyl ester resin with a glass fibre content of 75% by weight [12], whereas the BFRP bars were produced using a vinyl ester resin matrix with an estimated 75% fibre volume fraction [37]. Both bars were manufactured using a pultrusion process and had a nominal diameter of 8mm and 3mm respectively. The BFRP bars were mainly used to ease the building of the cages, and their contribution to ultimate capacity and overall structural behaviour can be considered to be negligible, yet resulting in a completely non-metallic reinforcing solution. Closed GFRP shear links with a rectangular cross section of 4x10mm were used as shear reinforcement over the shear spans (equally spaced at 100 mm), while steel stirrups were placed in proximity of both supports and loading points to prevent local crushing of concrete. No stirrups were provided in the pure bending zone.

Beams and tension stiffening specimens were cast in separate batches using the same mix design consisting of 358 kg/m^3 of cement type CEM I, 1000 kg/m^3 of coarse aggregate with a maximum size of 10 mm, 817 kg/m^3 of sand and a water/ cement ratio of 0.63 and 0.53, respectively. The average mechanical properties of the concrete used in this study are summarized in Table1 in terms of compressive strength, splitting tensile strength and modulus of elasticity, each determined by testing three samples and according to BS EN 12390-1, ASTM C496 and ASTM C469 [38-40], respectively. Concrete cubes and cylinders were cured under the same conditions as the test specimens (i.e., TS, BM) and tested on the same day as the corresponding specimens. It can be seen that a prolonged exposure to high temperature and high moisture levels can cause degradation in the concrete mechanical properties. This was also observed in previous studies (e.g. [41]). Ribbed GFRP bars with a nominal diameter of 8 mm were utilized in this study as tensile reinforcement for both TS and BM specimens. Table 2 summarizes the average values and associated standard deviations of the rupture tensile strength, f_{fu}, the modulus of elasticity, E_f, and the maximum strain, ε_{fu}, as obtained from uniaxial tension tests carried out on five samples according to ACI 440.3R-04 [34]. Nominal manufacturer values, when available, are provided in brackets.

The complete test matrix is presented in Table 3. Two replicate reference beams were unconditioned and unstressed. The remaining six beams were clamped in pairs back to back using an external rigid fixture consisting of transverse steel bolts and steel springs sandwiched between two steel plates as shown in (**Fig. 4**.-a). The desired sustained load was imposed by compressing the springs of a predetermined amount. A sustained stress inducing a tensile strain of 3000 με was selected as recommended by SLS design code provisions [24], while a higher stress inducing a strain of 5000 με was examined to assess the effect of less stringent serviceability limits. Beam specimens including 'W' in their designation were submerged in tap water at 60°C for 270 days to accelerate aging. During the conditioning period, the mid-span deformation of the beams was measured periodically using a caliper and demec gauge system. The crack width was measured using a hand-held microscope with a precision of 0.02 mm, whilst the sustained strain in the reinforcement was monitoring using strain gauges installed on each of the GFRP bars at mid-span.

As for the TS specimens, two replicate specimens were tested as reference, while the remaining were conditioned at 60°C and 100% relative humidity (RH) for 120 days. Two of these specimens were also stressed inducing a strain level of approximately 3000με in the reinforcement. The desired level of tensile strain in the TS specimens was applied via a spring of adequate stiffness mounted in a stiff pre-tensioning rig as shown in (**Fig. 4**-b).

2.1 **Tension stiffening specimens**

The TS specimens were tested with the setup shown in **Fig. 5** using a 1,000 kN ESH universal testing machine in displacement control, monitored through the internal transducer of the actuator, at a rate of 1 mm/min. Precautions were taken to avoid crushing of the bars in the machine grips. In particular, two threaded steel bars were drilled axially to obtain a hole in the longitudinal direction sufficiently large to accommodate the GFRP bar. These fixtures were mounted at both ends of the GFRP bars and bonded using epoxy resin. Each threaded steel bars was then embedded in two steel profiles and gripped in the machine (**Fig. 5**. A-A). **Fig. 5** also illustrates the layout of the potentiometers (P1 to P6) used to measure the average concrete deformation (P1 and P2, $dc_{concrete}$) and the average slip between the GFRP bar and the top (P3 and P4, $ds_{slip,top}$) and bottom (P5 and P6, $ds_{slip,bottom}$) surfaces of the concrete prism. Potentiometers P1 and P2 were placed on two slider joints bolted to the steel plates at both ends of the concrete prism, while potentiometers P3 to P6 were mounted on a plastic

collar coaxial to the GFRP bar and fixed to it with three equally-spaced screws at distance *dfe* from the end surfaces of the concrete prism.

In addition, deformations, crack width and spacing on a third face of the specimens were monitored using Digital Image Correlation (3D-DIC) to gain additional insights into the initiation and development of bond degradation. DIC is a contactless measuring technique for determining full-field deformations on the surface of an object under loading [42]. In this study, images were acquired with two CMOS digital cameras having a 4272×2848 pixel resolution (Canon EOS 1100D) and equipped with zoom lenses with F-number and focal length of 5.6 and 25 mm, respectively (Canon EF-S 18-55mm f/3.5-5.6 IS II). The cameras were rigidly connected 430 mm apart and mounted on a tripod. The stereo-vision system was positioned at 700 mm from the specimen. A light-emitting diode (LED) lamp was used to illuminate the measurement surface. During the test, the shutter was triggered remotely every 10 seconds by the data acquisition system in order to synchronize the images with point-wise transducers readings. The measured surface was smoothed and whitewashed to create a light background. A black speckle pattern was then spray-painted using a flexible stainless steel stencil. The target diameter of the speckles was approximately 1 mm in order to ensure an optimal speckle size of 4.5 pixels [43,44]

The measurements obtained from both LVDTs and DIC were used to determine the composite strain in the RC member and in the reinforcement, which are the key parameters governing tension stiffening response. The composite strain ($\varepsilon_{composite}$) is the strain in the portion of the bar originally embedded in concrete and it can be calculated by dividing the total measured elongation by the concrete length l_c. The total elongation is obtained as the concrete deformation (*dc*) plus the slip at the two ends of the prism (*ds*) discounted by the elastic deformation of the bar at the two ends of the specimen along (df_e) (Eq. 1).

$$\varepsilon_{composite} = \frac{Total\ elongation}{Concrete\ length} = \frac{dc + ds_{top} + ds_{bot} - \frac{Q}{A_f E_f}(2 * df_e)}{l_c} \quad (1)$$

where Q is the applied load; A_f is the area of the GFRP bar; and E_f is its modulus of elasticity and df_e is the gage length at both ends.

The concrete contribution (σ_c) is the tensile stress carried by the concrete as the applied load (Q) increases. This parameter has been used to evaluate the effect of the bar size on tension stiffening behaviour [45] and it will be employed in this study to assess the concrete tensile performances for different conditioning environments. The concrete contribution (σ_c) can be calculated based on equilibrium and assuming that the reinforcement strain (ε_f) is equal to the composite strain ($\varepsilon_{composite}$) (Eq. 2-4)

$$Q = Q_C + Q_f \quad (2)$$

$$Q_f = E_f . \varepsilon_f . A_f \quad (3)$$

$$\sigma_c = \frac{Q - E_f \varepsilon_f A_f}{A_c} \quad (4)$$

where Q is the applied load and Q_C and Q_f are the forces in the concrete and in the GFRP bar, respectively; and A_c is the area of the cross-section of the concrete prism.

The effect of sustained loading and environmental conditioning on the tension stiffening response will be assessed through the analysis of the tension stiffening performance factor (i_{TFP}) and the bond factor (β).

The tension stiffening performance factor (i_{TFP}) is determined by normalizing the concrete contribution with respect to the tensile cracking strength of the reference sample (f_{cr}) (Eq. 5).

$$i_{TFP} = \frac{\sigma_c}{f_{cr}} \quad (5)$$

The bond index represents the average load carried by the cracked concrete (Q_C) divided by the load carried by the concrete at first crack (Q_{Cr}) [46].

$$\text{bond index} = \frac{Q_C}{Q_{Cr}} \quad (6)$$

2.1.1 Analytical model for tension stiffening

The tension stiffening model adopted in *fib* model code 2010 [27], which was originally developed for steel RC, was shown to yield reliable results for the short-term tension stiffening behaviour of GFRP RC members [28]. According to this model, the strain behaviour is calculated in three stages, namely the uncracked stage, the crack formation stage and the stabilized cracking stage, according to (Eq. 7), (Eq. 8) and (Eq. 9), respectively.

Stage I (Uncracked): $$\varepsilon^*_{composite} = \frac{\sigma_c}{E_C} \quad (7)$$

Stage II (Crack formation): $$\varepsilon^*_{composite} = \frac{\sigma_{fr}.(1-\beta)}{E_f} \quad (8)$$

Stage III (Stabilized cracking): $$\varepsilon^*_{composite} = \frac{\sigma_f - \beta.\sigma_{fr}}{E_f} \quad (9)$$

Where, the maximum bar stress at a crack during stage II (σ_{fr}) can be defined according to Eq. 10

$$\sigma_{fr} = \frac{f_{ctm}}{\rho_{f.eff}}\left(1 + \alpha_c \rho_{f.eff}\right) \quad (10)$$

σ_f is the stress in the FRP bar at a crack; f_{ctm} is the tensile strength of the concrete; β is an empirical coefficient to assess the mean strain depending on the type of loading and can be either 0.6 for short-term loading or 0.4 for

long-term loading; $\rho_{f,eff}$ is the ratio between the cross-sectional area of bar and concrete; and α_c is the ratio between the modulus of elasticity of FRP and concrete.

2.2 Beams

Four-point bending tests were carried out using the set-up shown in **Fig. 2**. Beams were instrumented with linear variable differential transducers (LVDTs) at mid-span and at the supports to measure the net deflection. The load was applied in displacement control using a universal testing machine (1000 kN-ESH) at a rate of 1 mm/min, monitored through the internal transducer of the actuator. Quasi-static incremental loading cycles were carried out at a load inducing a predefined level of strain in the tensile reinforcement, namely 3000 με and 5000 με, before the beams were loaded to failure. Crack widths were also measured at every 5 kN load increment with a crack width microscope.

2.2.1 Review of EC2 and ACI 440.1R-15 models to predict deflection

According to Eurocode 2 [47], the total deformations (curvature or deflection) of members subjected to flexure can be calculated by an interpolation between cracked and un-cracked section deformations (Eq.11), which is conceptually more meaningful to represent the variation of the stiffness along the length of the beam due to the presence of cracking [11,19].

$$\alpha = \zeta.\alpha_{II} + (1-\zeta).\alpha_{I} \quad (11)$$

$$\zeta = 1-\beta\left(\frac{M_{cr}}{M}\right)^2 \quad (12)$$

where α is the considered deformation parameter (e.g. deflection) and the subscripts I and II refer to un-cracked and cracked states, respectively; ζ is a distribution coefficient (accounting for tensioning stiffening response of the RC member at a section); β is a load duration coefficient (1 for short-term loading and 0.5 for sustained or repeated loading); M_{cr} is the cracking moment; and M is the applied moment.

ACI 440.1R-15 [24] recommends the use of an effective moment of inertia, I_{eff}, derived from a modification of Branson's equation (Eq. 13):

$$I_e = \left(\frac{M_{cr}}{M_a}\right)^3 \beta_d I_g + \left[1 - \left(\frac{M_{cr}}{M_a}\right)^3\right] I_{cr} \leq I_g \quad (13)$$

$$\beta_d = \frac{1}{5}\left(\frac{\rho_f}{\rho_{fb}}\right) \leq 1.0 \quad (14)$$

$$\rho_{fb} = 0.85\beta_1 \frac{f_c'}{f_{fu}} \frac{E_f \varepsilon_{cu}}{f_{fu}E_f + f_{fu}} \quad (15)$$

where β_d is a coefficient accounting for the different tension stiffening behaviour of FRP RC elements; ρ_f is the FRP reinforcement ratio and ρ_{fb} is the FRP balanced reinforcement ratio; β_1 is the ratio between the height of the equivalent rectangular stress block and the neutral axis depth; f'_c is the concrete compressive strength, f_{fu} is the rebar tensile strength, E_f is the modulus of elasticity of the FRP rebar, and ε_{cu} is the maximum concrete strain (0.003 according to ACI provisions).Review of EC2 and ACI code to predict maximum crack width and spacing

EC2 calculates the maximum crack width and the maximum crack spacing according to Eq. 16 and Eq. 17, respectively.

$$w_{cr,max} = S_{cr,max}(\varepsilon_{fm} - \varepsilon_{cm}) \quad (16)$$

$$S_{cr,max} = 3.4c + 0.425k_1k_2\emptyset/\rho_{p,eff} \quad (17)$$

$$(\varepsilon_{fm} - \varepsilon_{cm}) = \frac{\sigma_f}{E_f} - \frac{k_t f_{ct,eff}(1+\alpha_c\rho_{p,eff})}{E_f\rho_{p,eff}} \geq 0.6\frac{\sigma_f}{E_f} \quad (18)$$

where $S_{cr,max}$ is the maximum crack spacing; c is the concrete cover; k_1 is the bond coefficient equal to 0.8 for good bond performance and 1.6 for low bond performance; k_2 is a coefficient depending on the form of the strain distribution (0.5 for bending and 1 for pure tension); Ø is the diameter of the bar; $\rho_{p,eff}$ is the effective reinforcement ratio, where the effective area of the concrete in tension is calculated according to Eq. 16

$$A_{eff} = min\left\{2.5b.(h-d), \frac{b(h-x)}{3}, \frac{bh}{2}\right\} \quad (19)$$

h and b are the width and the height of the beam; d is the effective depth; and x is the neutral axis depth.

The mean differential strain (ε_{fm}-ε_{cm}) can be calculated according to Eq. 18 as the difference between the strain in the reinforcement, ε_{fm}, and the mean concrete strain, ε_{cm}, between cracks, which takes into account the tension stiffening effect; the stress in the tension reinforcement, σ_f, is calculated by assuming a cracked section; k_t is a factor depending on the duration of the loading (0.6 for short-term loads and 0.4 for long-term loading); and $f_{ct,eff}$ is the effective concrete tensile strength

ACI440.1R-15 recommends using Eq. 20 to estimate the maximum probable crack width in FRP reinforced concrete elements

$$w = 2\frac{f_f}{E_f}\beta_c k_b \sqrt{d_c^2 + \left(\frac{s}{2}\right)^2} \quad (20)$$

where, σ_f is the tensile stress in the reinforcement; E_f is the elastic modulus of the reinforcement; $\beta_c = (h-x)/(d-x)$; d_c is the cover thickness from the tension face to the centre of the closest reinforcing bar; and s is the bar spacing. The k_b is a coefficient accounting for the bond behaviour between FRP bar and concrete. The bond coefficient k_b is taken as 1 for FRP bars having similar bond behaviour to conventional steel bars. However, if the k_b value is not known, a conservative value of 1.4 is recommended.

3 Experimental results and discussion

The experimental results are presented in the following sections and are used to discuss the effect of long-term environmental exposure on the tension stiffening and flexural behaviour of the tested specimens.

3.1 Tension stiffening response of GFRP RC specimens

The effect of environmental long-term exposure and sustained stress on the tension stiffening behaviour can be evaluated by analysing the load–strain responses, the cracking behaviour and the concrete contribution.

3.1.1 Load–strain responses

Fig. 6 presents the load–strain responses measured during the experimental tests for the reference specimens and for those conditioned in water at 60°C for 120 days with and without sustained loading. The composite strains ($\varepsilon_{composite}$) were computed according to Eq.1, and, for comparison purposes, the fully cracked response (unconditioned bare GFRP bar) is also plotted. The graph shows that the unstressed conditioned specimens (TS3.120.60.W and TS4.120.60.W) exhibited significantly higher tension stiffening than the stressed specimens (TS5.120.60.W.3k and TS6.120.60.W.3k). This suggests that, in unstressed specimens, the bond between the bar and the concrete increased, possibly due to the swelling of the bar due to moisture absorption and to the resulting increase in mechanical interlocking and in friction forces at the interface (**Fig. 7)** [33]. Conversely, specimens conditioned under sustained stress had a relatively lower tension stiffening response after cracking compared to other specimens and an initial softer response up to cracking load. This is supported also by examining the variation of the bond index (Eq. 6) with increasing $\varepsilon_{composite}$ (**Fig. 8**) and by estimating the tension stiffening as the normalised area under each curve (A_1, A_2 and A_3). The observed bond enhancement for unstressed specimens was approximately 43% compared with the references specimens, whilst stressed conditioned samples exhibited a decrease in tension stiffening of approximately 7%. This reduction might be due to the development of micro-cracks as a result of concrete creep and to the deterioration of the resin rich layer of the bars in moist concrete environment, leading to bond degradation and to the consequent slipping of

the bar at both ends of the specimens. Evidence of slip between the bar and the concrete was also evident when specimens were subsequently split for closer investigation. Residues of the ribs of the GFRP bar were found encased in the concrete at the two ends of the specimen (**Fig.** -a-c), confirming that failure developed at the interface layer between the ribs and the core of the bar.

The performance of *fib* 2010 in predicting the tension stiffening response of conditioned the GFRP RC members is presented in **Fig. 10** (a) and (b) respectively. The bare bar response is also included for reference. While the general trend is well captured, the model significantly underestimates the deformation of both reference and stressed specimens, while it underestimates the tension stiffening behaviour of the unstressed specimens.

3.1.2 Concrete contribution

Fig. 11 shows the variation of the tension stiffening performance indexes (i_{TSP}, see Eq.5) of both unconditioned and conditioned TS specimens as a function of composite strain ($\varepsilon_{composite}$, Eq. 1). The areas under each curve, which are also reported in **Fig. 11** and are here referred to as the tension stiffening performance values, were calculated and compared to examine the concrete contribution to the overall tensile response. The tension stiffening performance of unstressed specimens conditioned in water at 60°C increased approximately by 88% compared to that of the reference specimens, whereas a decrease of approximately 15% was recorded in the stressed samples. Similarly, the experimental concrete contribution at cracking load, σ_c, calculated according to Eq. 4 and summarized in Table 4, shows on average an increase of approximately 36% for the unstressed specimens and a decrease of approximately 16% for the stressed samples when compared to the control specimens. These results are in line with the observations made above in reference to the bond enhancement found in unstressed samples and the tension stiffening degradation seen in stressed specimens. As evidenced in **Fig. 9**-b, the presence of a sustained load caused local de-bonding along the bar, thus affecting the overall bond and tension stiffening behaviour.

3.1.3 Cracking behaviour

Typical crack patterns just before failure are presented in **Fig. 12**, in which cracks can be identified as a sudden increment in the vertical displacement field (i.e. sharp change in colour) captured through DIC. The number associated with each crack represents their order of appearance, while the numbers between cracks are the measured spacing values. Unstressed conditioned specimens exhibited a smaller average crack spacing (60mm) and a higher number of cracks (4) than stressed specimens, characterized by an average crack spacing of 169mm and two primary cracks, and also than reference specimens that had an average crack spacing of 88 mm and three primary cracks. This suggests that the unstressed conditioned specimens had a better bond compared to the

others tested specimens and corroborates the observations made above on bond enhancement in unstressed specimens, which resulted in a more effective stress transfer from the bar to the concrete and consequently in the opening of a higher number of cracks. Conversely, the bond degradation in stressed specimens reduced the stress transferred to the concrete and therefore the number of cracks.

3.2 Load test of small-scale GFRP RC beams

The results of four-point bending tests on small-scale GFRP RC beams are discussed below in terms of load-deflection response as well as cracking behaviour. The results from the study on the tensile behaviour of conditioned and stressed GFRP bars embedded in concrete are also used in the following to gain additional insights on the overall performance of GFRP RC elements.

3.2.1 Load-deflection behaviour

Fig. 13 shows typical experimental load–deflection curves for specimens subjected to each type of conditioning and sustained loading, along with the theoretical response obtained by implementing the EC 2 and ACI 440.1R-06 models. It should be noted that the overall experimental deflection shown in the figure also includes the residual deformation due to the applied sustained load (initial offset at zero load). As the design of GFRP RC members is usually controlled by SLS limitations, the test results were compared at service load, which corresponds, as recommended by EC2, to about 35% of the ultimate load (ULS) of BM1.REF (shown in the figure with an horizontal solid line). In particular, it was observed that specimens conditioned in water at 60°C and with sustained loading corresponding to 3000 με and 5000 με showed larger deformations (up to 49% and 68%, respectively) than BM1.REF. Such increments may be attributed to the reduction in tension stiffening effect as observed in the direct tension tests previously discussed. It could be also attributed to the degradation of concrete properties as a result of the exposure to warm and humid conditions. While the deflection of the stressed beam conditioned at ambient temperature (BM3.270.20.a.3k) is similar to the one of the control beam, a reduction in stiffness was noticed at early stages of loading, which was fully recovered once the load reached about 6 kN. This could be attributed to a local bond degradation between bars and concrete at the crack locations due to creep of concrete over the period that the specimens were subjected to the sustained load. Conversely, beams conditioned in water showed some high initial stiffness at early stage of loading that could be attributed to the self-heling phenomenon typical of concrete in wet conditions.

Fig. 13-a and **Fig. 13**-b show that the EC2 model predicted with a good degree of accuracy the deflections of the control beam and the stressed beam conditioned at ambient temperature up to service load. However, for load levels higher than 30 kN, the model underestimated the deflections, not accounting for the contribution of shear cracks to the total deformation. In addition, despite providing sufficiently accurate predictions at service load for short and long term conditioning at ambient temperature, the EC2 model significantly underestimated deflection for specimens subjected to long-term conditioning in water at 60°C. While ACI 440 significantly underestimated the predicted deflections for all cases, possibly because the tension stiffening effect was overestimated. It can also be noted that, only beam BM7.270.60.W.5k deflected more than the maximum allowable deflection at SLS (taken as *l*/250, or 4 mm) and highlighted in **Fig. 13** with a vertical solid line.

3.2.2 Crack spacing

The cracking patterns for all tested beams at SLS and at ULS are shown in **Fig. 14** and **Fig. 15**, respectively. Initially, vertical cracks appeared in the pure bending zone as the load reached the cracking level for the reference specimens (un-cracked before testing) which were 9.06 and 10.34 kN, for BM1.REF and BM2.REF respectively, and as it exceeded 5 kN for the conditioned specimens (pre-cracked due to imposed sustained stress). As the load approached 20 kN shear cracks begun to form. It was noted that conditioned beams developed fewer secondary cracks than control beams as the bond between GFRP bars and concrete deteriorated during the conditioning process. The number of primary cracks as well as the average and the maximum crack spacing at both SLS and ULS are presented in Table 5 along with the maximum experimental load capacity and the theoretical maximum crack spacing values calculated considering both good and poor bond conditions (i.e., k_1=0.8. and k_1=1.6, respectively). The control beams consistently showed the lowest average crack spacing both at SLS and at ULS, confirming the good bond of unconditioned GFRP bars with concrete. The effect of sustained stress on crack spacing was variable and difficult to decouple from the influence of the moist alkaline environment at high temperature. In general, the wider crack spacing in stressed beams conditioned in water can be attributed to the reduction in bond strength as result of the skin degradation of the bars. Based on the outcomes of the tension stiffening results, the theoretical value representing good bond is adopted to predict the maximum crack spacing of reference specimens, whereas the one representing poor bond is used in the case of stressed specimens.

The crack spacing obtained from EC2 is in good agreement with the test results at SLS. In particular, at SLS, the crack spacing predicted for beams BM4.270.60.a.3k and BM7.270.60.W.5k are slightly overestimated.

3.2.3 Crack width

The width of the cracks that developed within the constant bending moment zone was measured at the height of the longitudinal reinforcement at different load levels using an optical microscope. **Fig. 16** shows the experimental crack widths for one of the specimens subjected to each type of conditioning environment and sustained loading as well as the predicted crack widths according to EC2 and ACI 440. In general, crack widths were larger for stressed samples conditioned in water at high temperature. Nonetheless, for all specimens, the maximum measured crack width at SLS always remained within the allowable crack width (i.e. 0.5 mm) according to current guidelines [24-25]. It can be noted that the experimental maximum crack width of the control beam can be accurately predicted by the EC2 approach with a bond coefficient of 0.8, as no onset bond degradation is expected at this stage. However, the model fails to predict accurately the crack widths for the conditioned and stressed specimens, providing conservative values for dry environments while being un-conservative for exposure to wet conditions. Similarly to EC2, despite using the recommended conservative value for the bond factor, ACI 440.1R-15 fails to capture the behaviour of stressed specimens conditioned in water. It should also be noted that the ACI model does not include a time dependent factor. Thus, using short-term tests results to predict the long-term cracking response of GFRP RC members and develop service life prediction models can lead to an unsafe design.

4 Conclusions

The experimental data obtained from this research was used to examine the long-term performance of GFRP bars in concrete members and assess the performance of the *fib* and EC2 models for predicting tension stiffening, deflections as well as crack spacing and crack width. The results of this study are summarized below.

- Exposure to severe environment and sustained loading deteriorated the resin rich layer of GFRP bars. This resulted in the bond degradation between concrete and reinforcement and, in turn, reduced tension stiffening and affected the total structural performance of the GFRP RC members. Conversely, exposure to a moist environment without sustained loading did not cause any noticeable bond strength degradation. In fact, the swelling of the GFRP bar, as a result of moisture absorption, increased the mechanical interlocking and the friction forces at the interface between concrete and reinforcement, leading to a stronger bond and to a relatively higher tension stiffening behaviour.
- The *fib* model failed to accurately represent the tension stiffening response of the tested GFRP RC members. In particular, the model underestimated the performance of the unstressed conditioned

specimens while, overestimated that reference and stressed conditioned specimens. Additional work is recommended to further improve the accuracy of this model.

- The deformations (deflection and crack width) of the beams subjected to a load that induced strain levels of about 3000με in the GFRP bars remained within the limiting values suggested in current guidelines. Only the beams subjected to a higher sustained load level (equivalent to a strain of 5000με in the GFRP bars) exhibited deformations exceeding current allowable limits.
- Current models to predict deflection and crack width failed to capture adequately the combined effect of severe environment and sustained loading. In particular, the EC2 model predictions were in agreement with the experimental deflection results measured at service load for reference specimens (short-term) and for stressed beams that were conditioned in air (long-term). However, the predicted deformation for stressed beams that were conditioned in water (long-term) was significantly underestimated by both EC2 and ACI 440. In addition, the use of a bond coefficient describing weak bond conditions led to unsafe crack width predictions. More accurate tension stiffening and bond factors representing GFRP RC beams in real application need to be identified.

It should be mentioned that the above conclusions are based on the analysis of test results carried out on a single type of GFRP bar and a limited number of specimens and conditioning environments thus may not directly extend to other types of reinforcement or environmental conditions. Additional tests should be performed to provide statistically significant results and conclusions.

5 Funding

This work was financially supported by The University of Benghazi.

6 Acknowledgements

The authors gratefully thank the staff of the heavy structure laboratory of the University of Sheffield for their assistance.

7 References:

1. Nkurunziza, G., Debaiky, A., Cousin, P. and Benmokrane, B., 2005. Durability of GFRP bars: a critical review of the literature. *Progress in structural engineering and materials*, *7*(4), pp.194-209.

2. Benmokrane, B. and Mohamed, H.M., 2013, J. Durability issues of FRP for civil infrastructure. In *11th international symposium on fiber reinforced polymers for reinforced concrete structures (FRPRCS11). Guimaraes*.

3. Micelli, F. and Nanni, A., 2004. Durability of FRP rods for concrete structures. *Construction and Building materials*, *18*(7), pp.491-503.

4. Nanni, A., Claure, G., y Basalo, F.J.D.C. and Gooranorimi, O., 2016. Concrete and Composites Pedestrian Bridge. Concrete International, 38(11), pp.57-63.

5. Miàs, C., Torres, L., Turon, A. and Barris, C., 2013. Experimental study of immediate and time-dependent deflections of GFRP reinforced concrete beams. *Composite Structures*, *96*, pp.279-285.

6. Kara, I.F. and Ashour, A.F., 2012. Flexural performance of FRP reinforced concrete beams. *Composite Structures*, 94(5), pp.1616-1625.

7. Qin, R., Zhou, A. and Lau, D., 2017. Effect of reinforcement ratio on the flexural performance of hybrid FRP reinforced concrete beams. *Composites Part B: Engineering*, 108, pp.200-209.

8. Pecce, M., Manfredi, G. and Cosenza, E., 2000. Experimental response and code Modelsof GFRP RC beams in bending. *Journal of Composites for Construction*, *4*(4), pp.182-190.

9. Toutanji, H.A. and Saafi, M., 2000. Flexural behavior of concrete beams reinforced with glass fiber-reinforced polymer (GFRP) bars. *ACI structural journal*, *97*(5), pp.712-719.

10. Yost, J.R., Gross, S.P. and Dinehart, D.W., 2003. Effective moment of inertia for glass fiber-reinforced polymer-reinforced concrete beams. *Structural Journal*, *100*(6), pp.732-739.

11. Bischoff, P.H., 2005. Reevaluation of deflection prediction for concrete beams reinforced with steel and fiber reinforced polymer bars. *Journal of Structural Engineering*, *131*(5), pp.752-767.

12. Barris, C., Torres, L., Turon, A., Baena, M. and Catalan, A., 2009. An experimental study of the flexural behaviour of GFRP RC beams and comparison with prediction models. *Composite Structures*, *91*(3), pp.286-295.

13. Almusallam, T.H. and Al-Salloum, Y.A., 2006. Durability of GFRP rebars in concrete beams under sustained loads at severe environments. Journal of composite materials, 40(7), pp.623-637

14. Park, Y., Kim, Y.H. and Lee, S.H., 2014. Long-term flexural behaviors of GFRP reinforced concrete beams exposed to accelerated aging exposure conditions. *Polymers*, 6(6), pp.1773-1793.

15. Park, Y., 2012. Long-Term Performance of GFRP Reinforced Concrete Beams and Bars Subjected to Aggressive Environments. *Texas A&M University*, Ph.D Dissertation

16. Kassem, C., Farghaly, A.S. and Benmokrane, B., 2011. Evaluation of flexural behavior and serviceability performance of concrete beams reinforced with FRP bars. *Journal of Composites for Construction*, *15*(5), pp.682-695.

17. Benmokrane, B., Chaallal, O. and Masmoudi, R., 1996. Flexural response of concrete beams reinforced with FRP reinforcing bars. *ACI Structural Journal*, *93*(1), pp.46-55.

18. Masmoudi, R., Theriault, M. and Benmokrane, B., 1998. Flexural behavior of concrete beams reinforced with deformed fiber reinforced plastic reinforcing rods. *Structural Journal*, *95*(6), pp.665-676.

19. Barris, C., Torres, L., Baena, M., Pilakoutas, K. and Guadagnini, M., 2012. Serviceability limit state of FRP RC beams. *Advances in Structural Engineering*, *15*(4), pp.653-663.

20. Faza, S. S., and GangaRao, H. V. S. 1992. "Pre- and post-cracking deflection behavior of concrete beams reinforced with fiber-reinforced plastic rebars." *Proc., 1st Int. Conf. on the Use of Advanced Composite Materials in Bridges and Structures (ACMBS-I)*, K. Neale and P. Labossiere, eds., Society for Civil Engineering, Montreal, Canada, 151–160

21. Mota, C., Alminar, S., and Svecova, D. 2006. "Critical review of deflection formulas for FRP-RC members." *J. Compos. Constr., 10(3*), 183–194.

22. Razaqpur, A. G., Svecova, D., and Cheung, M. S. 2000. "Rational method for calculating deflection of fiber-reinforced polymer reinforced beams." *ACI Struct. J*., 97(1), 175–184.

23. Bischoff, B. H., and Scanlon, A. 2007. "Effective moment of inertia for calculating deflections of concrete members containing steel reinforcement and fiber-reinforced polymer reinforcement." *ACI Struct. J*., 104(1), 68–75.

24. ACI (American Concrete Institute). 2015. Guide for the design and construction of concrete reinforced with FRP bars. *ACI 440.1R-15, Farmington Hills*, MI.

25. Canadian Standards Association, CSA., 2002. Design Construction of Building Components with Fibre-Reinforced Polymers. *CSA S806–02, Canadian Standards Association, Rexdale, Ont., Canada*.

26. Italian National Research Council (CNR). 2006. Guide for the design and construction of concrete structures reinforced with fiber-reinforced polymer bars, *CNR-DT 203/2006, Rome*

27. Model Code, 2010. First complete draft–vol. 1. *fib Bulletin*, (55).

28. Kharal, Z. and Sheikh, S., 2017. Tension Stiffening and Cracking Behavior of Glass Fiber-Reinforced Polymer-Reinforced Concrete. *ACI Structural Journal*, *114*(2), p.299.

29. Bischoff, P.H. and Paixao, R., 2004. Tension stiffening and cracking of concrete reinforced with glass fiber reinforced polymer (GFRP) bars. *Canadian Journal of Civil Engineering*, *31*(4), pp.579-588.

30. Scott, R.H. and Beeby, A.W., 2005. Long-term tension-stiffening effects in concrete. *ACI Structural Journal*, *102*(1), p.31.

31. Fergani, H., Di Benedetti, M., Mias, C., Lynsdale, C. and Guadagnini, M.,2016. Characterization and durability study of GFRP bars exposed to severe environments and under sustained loads. In *Proceedings The 5th International Conference on Durability of Fibre Reinforced Polymer (FRP) Composites for Construction and Rehabilitation of Structures, Sherbrooke, Canda*

32. Elbadry, M.M., Abdalla, H. and Ghali, A., 2000. Effects of temperature on the behaviour of fiber reinforced polymer reinforced concrete members: experimental studies. *Canadian Journal of Civil Engineering*, *27*(5), pp.993-1004.

33. Fergani, H., Di Benedetti, M., Mias, C., Lynsdale, C. and Guadagnini, M.2016. Long-term performance of GFRP bars under the combined effects of sustained load and severe environments. *In Proceedings the 8th International Conference on Fibre-Reinforced Polymer (FRP) Composites in Civil Engineering*, Hong Kong, China

34. ACI, A., 2004. 440.3 R-04: Guide Test Methods for Fiber-Reinforced Polymers (FRPs) for Reinforcing or Strengthening Concrete Structures. *American Concrete Institute, Farmington Hills, USA*.

35. Robert, M., Wang, P., Cousin, P. and Benmokrane, B., 2010. Temperature as an accelerating factor for long-term durability testing of FRPs: Should there be any limitations?. *Journal of Composites for Construction*, 14(4), pp.361-367.

36. Davalos, J.F., Chen, Y. and Ray, I., 2012. Long-term durability prediction models for GFRP bars in concrete environment. *Journal of Composite Materials*, 46(16), pp.1899-1914.

37. Serbescu, A., Guadagnini, M. and Pilakoutas, K., 2014. Mechanical characterization of basalt FRP rebars and long-term strength predictive model. *Journal of Composites for Construction*, 19(2), p.04014037.

38. EN, BS., 2012. 12390-1: Testing hardened concrete Shape, dimensions and other requirements for specimens and moulds. *British Standards Institute, London*.

39. ASTM C496/C496M-11, Standard test method for splitting tensile strength of cylindrical concrete specimens.

40. ASTM C469-94,. Standard Test Method for Static Modulus of Elasticity and Poisson's Ratio of Concrete in Compression. 1994

41. Shoukry, S.N., William, G.W., Downie, B. and Riad, M.Y., 2011. Effect of moisture and temperature on the mechanical properties of concrete. *Construction and Building Materials*, 25(2), pp.688-696.

42. Sutton, M.A., 2013. Computer vision-based, noncontacting deformation measurements in mechanics: a generational transformation. *Applied Mechanics Reviews*, *65*(5), p.050802.

43. Zappa, E., Mazzoleni, P. and Matinmanesh, A., 2014. Uncertainty assessment of digital image correlation method in dynamic applications. *Optics and Lasers in Engineering*, *56*, pp.140-151.

44. Di Benedetti, M., Cholostiakow, S., Fergani, H., Zappa. E., Cigada, A., and Guadagnini, M., 2015. 3D-DIC for strain measurement in small scale GFRP RC specimens. *Third Conference on Smart Monitoring, Assessment and Rehabilitation of Civil Structures*, Antalya, Turkey

45. Sooriyaarachchi, H., Pilakoutas, K. and Byars, E., 2005. Tension stiffening behavior of GFRP-reinforced concrete. *In proceedings of the Seventh International Symposium of Fiber-Reinforced Polymer Reinforcement for Reinforced Concrete Structures (FRPRCS-7), Kansas City, Missouri*

46. Bischoff, P.H., 2001. Effects of shrinkage on tension stiffening and cracking in reinforced concrete. *Canadian Journal of Civil Engineering*, *28*(3), pp.363-374.

47. British Standards Institution, 2004. Eurocode 2: Design of Concrete Structures: Part 1-1: General Rules and Rules for Buildings. British Standards Institution.

Figures

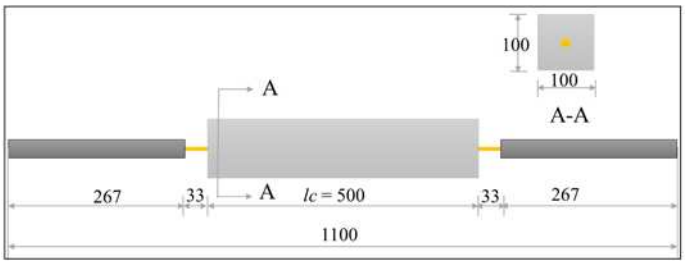

543

544 **Fig. 1: Geometric details of the Tension stiffening specimens (all dimensions in mm)**

545

546

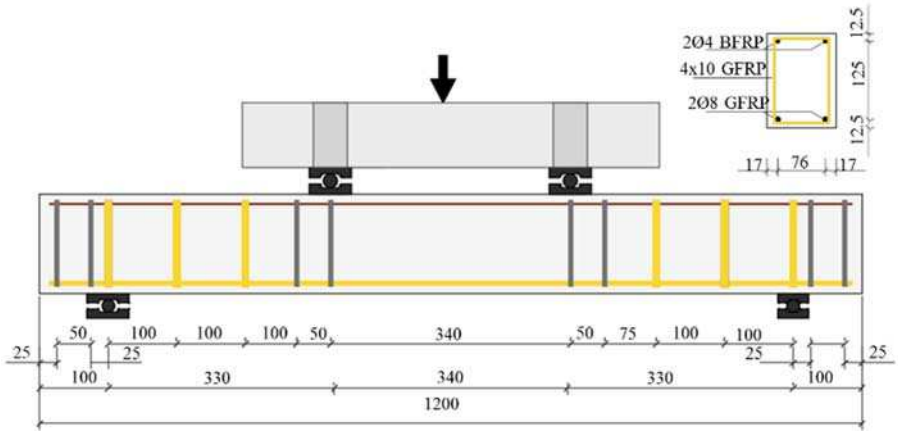

547
548 **Fig. 2: Geometric details and test setup of the tested FRP RC beams (all dimensions in mm)**

549

550

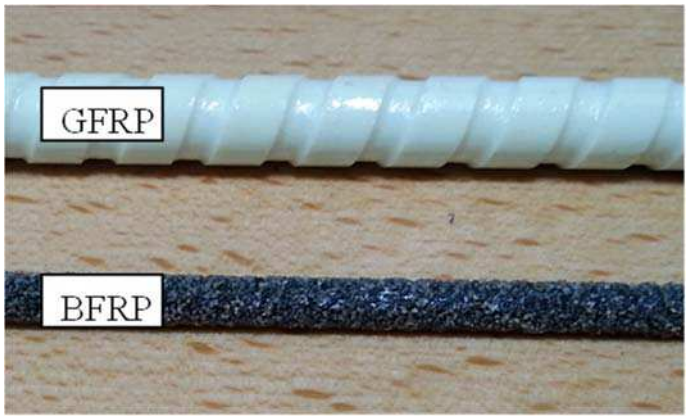

551
552 **Fig. 3: Surface deformations and characteristics of rebars**

553

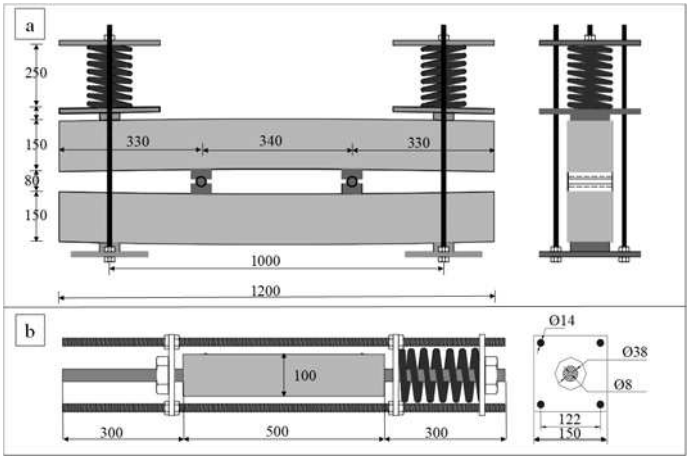

554
555 **Fig. 4: sustained load for simulating service loading (a) on beams (b) on tension stiffening specimens (all**
556 **dimensions in mm)**

557

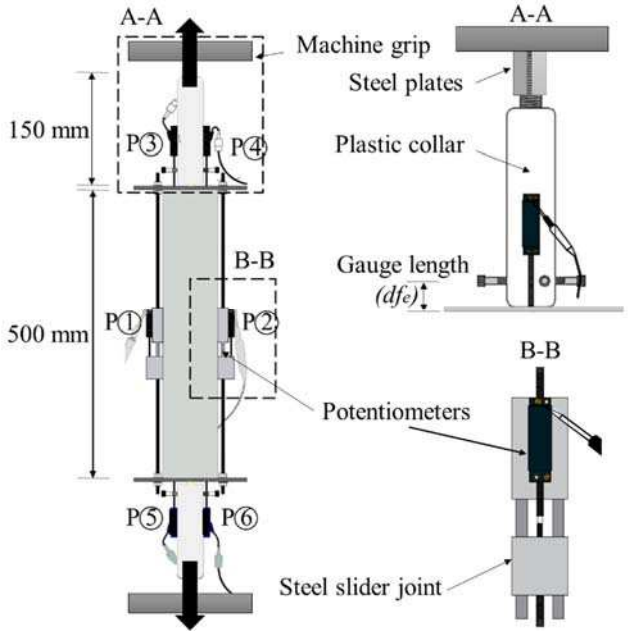

558

559 **Fig. 5: Test set-up for direct tension test**

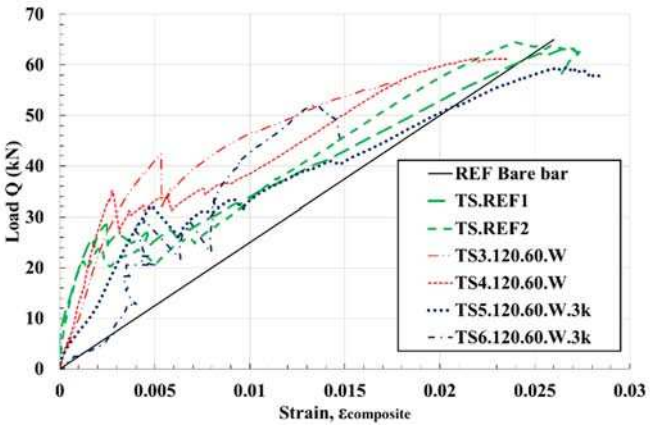

560
561 **Fig. 6: Composite responses against applied load**

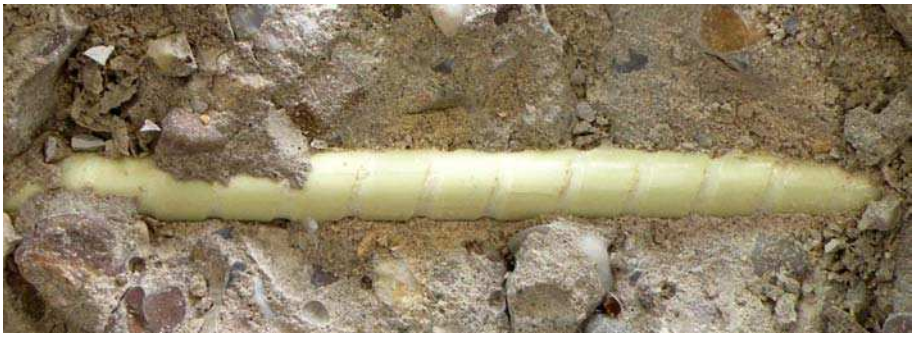

562
563 **Fig. 7: Extracting the bars from conditioned unstressed specimens**

564

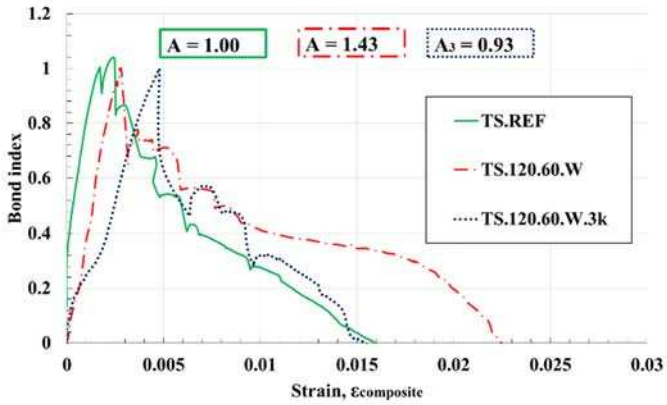

565
566 **Fig. 8: Tension-stiffening bond index response $A_{1,2,3}$ are the area under each curve.**

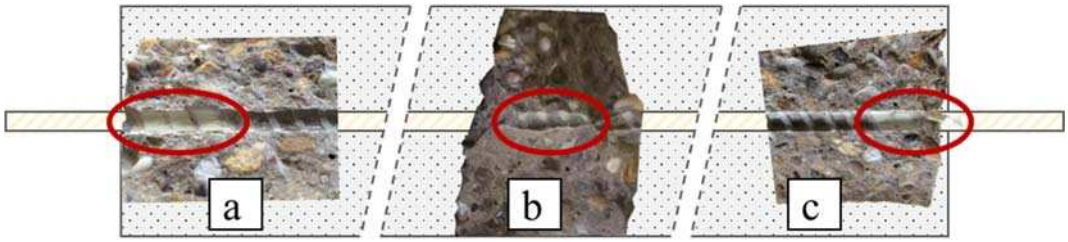

567
568 **Fig. 9: ribs rupture and surface degradation in stressed specimens.**

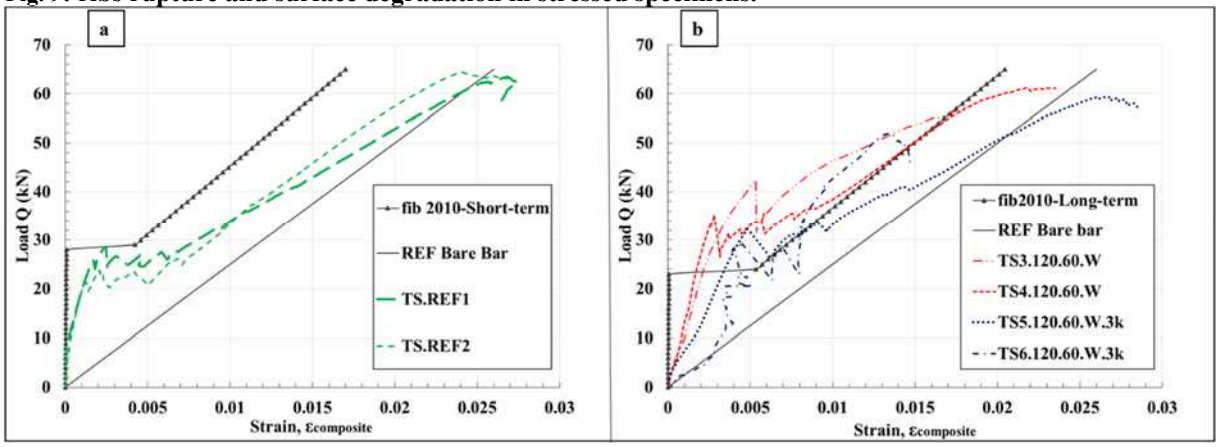

569

570 **Fig. 10: (a) short-term prediction and the corresponding test results for references (b) long-term**
571 **prediction and the corresponding test results aged specimens**

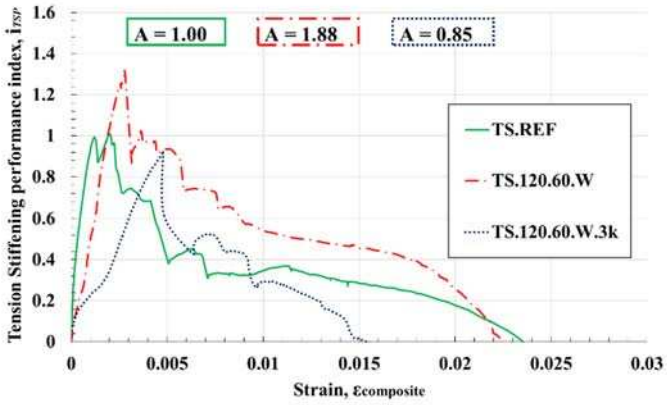

572
573 **Fig. 11: Tension stiffening contribution**

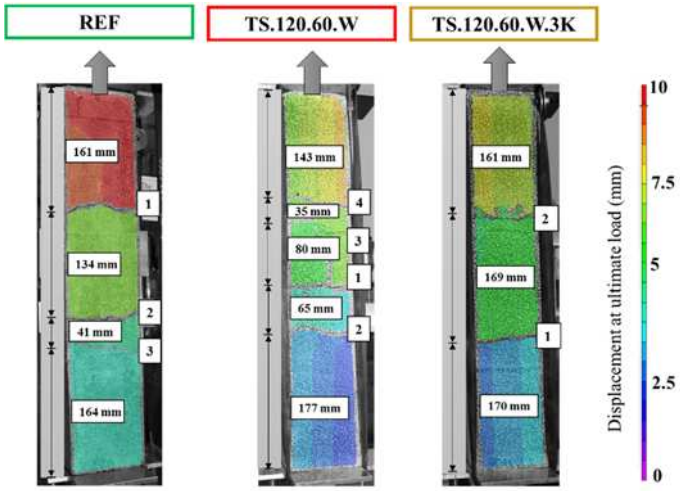

574
575 **Fig. 12: Displacement measurement by DIC, crack spacing and the crack number according to the**
576 **appearance**

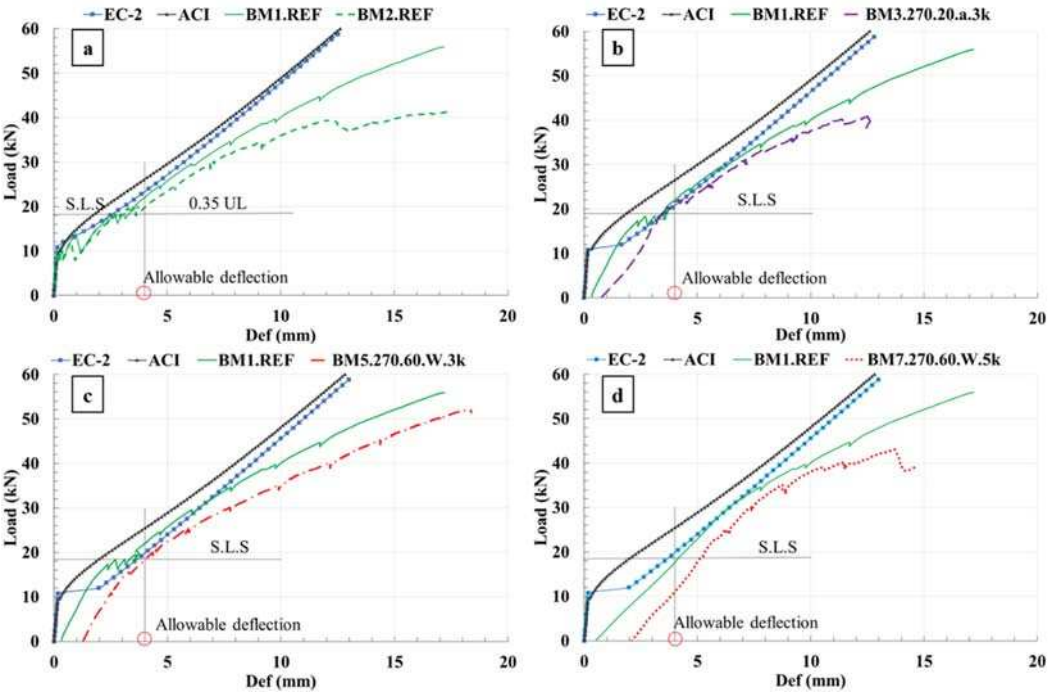

577
578 **Fig. 13: Theoretical and experimental load-deflection curves: (a) Control beams; (b) 3000με stressed**
579 **beams aged in air; (c) 3000με stressed beams aged in tank; (d) 5000με beams tank**

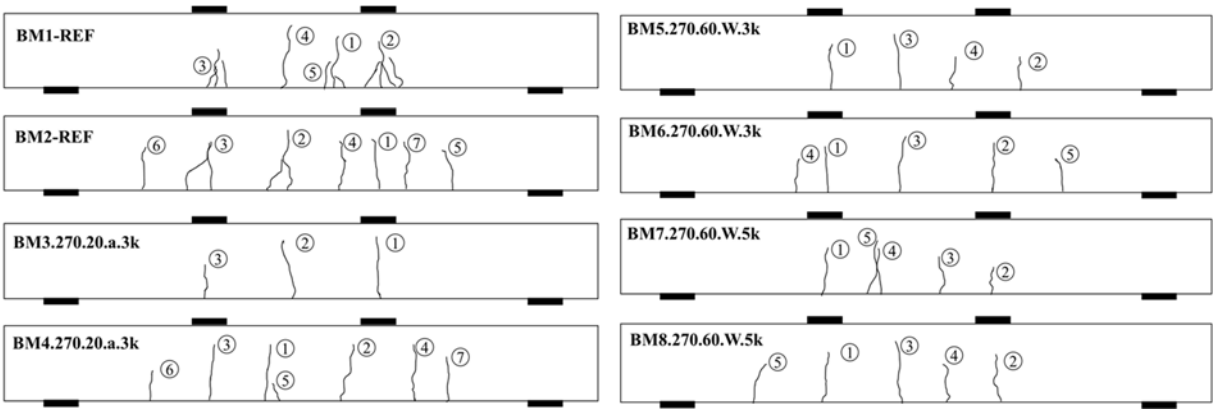

Fig. 14: Crack pattern at service load of tested beams

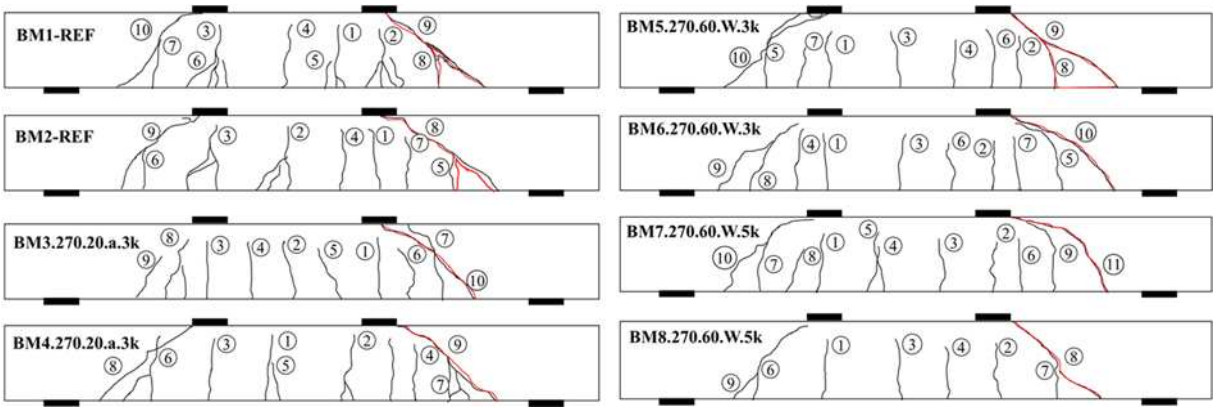

Fig. 15: Crack pattern at failure of tested beams the red coulure is failure crack.

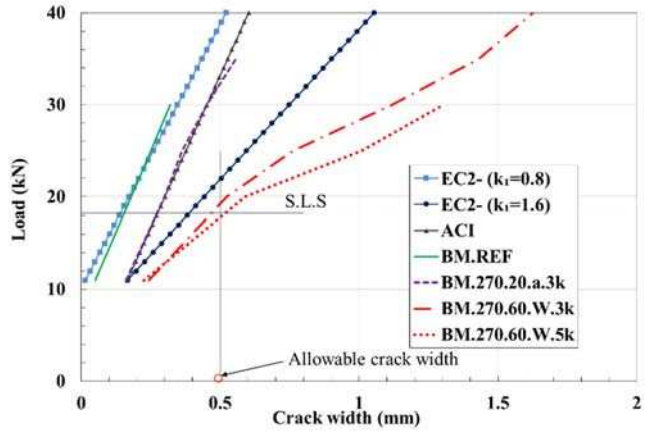

Fig. 16: Crack width vs. applied load compared with EC2 model.

Table 1. Concrete properties

Sample	Curing environment			f_c		E_C		f_{ct}	
	RH (%)*	Temperature (°C)	Time (days)	Avg (MPa)	St.D	Avg (GPa)	St.D	Avg (MPa)	St.D
BM	RH 80%	20	0	55.0	1.4	33.1	0.4	3.2	0.2
BM	RH 100%	60	270	35.5	3.9	26.2	3.5	2.6	0.5
BM	RH 50%	20	270	50.4	8.4	33.1	2.1	3.0	0.3

TS	RH 80%	20	0	60.5	5.2	33.8	1.0	3.6	0.3
TS	RH 100%	60	120	52.0	6.0	32.7	1.8	3.0	0.1

590 *RH Relative humidity

591 **Table 2. Reinforcement material properties.**

Reinforcement			E_f		ε_{fu}		f_{fu}	
Type	Material	Size (mm)	Avg. (GPa)	St.D. (GPa)	Avg. (%)	St.D. (%)	Avg. (MPa)	St.D. (MPa)
Tension	GFRP	Ø8	57.0 (60.0)	1.5	2.8	0.9	1542.0 (1000.0)	28.0
Compression	BFRP	Ø4	44.0	1.0	2.9	_	1285.0	47.0
Shear	GFRP	4x10	28.0	_	1.9	_	720.0	_

592

593 **Table 3. Test matrix and environmental and mechanical conditioning parameters.**

Specimen*		Conditioning			Applied strain in longitudinal reinforcement (με)
Label	Test	Environment	Temperature (°C)	Time (d)	
TS.REF	TS	Laboratory	20	0	0
TS.120.60.W	TS	100% RH	60	120	0
TS.120.60.W.3k	TS	100% RH	60	120	3000
BM.REF	FLX	Laboratory	20	270	0
BM.270.20.a.3k	FLX	Laboratory	20	270	3000
BM.270.60.W.3k	FLX	Tap Water	60	270	3000
BM.270.60.W.5k	FLX	Tap Water	60	270	5000

594 * two replicates of each specimen were tested

595 **Table 4. Concrete contribution in tensile behaviour**

specimens	Concrete contribution at cracking load		$\sigma_c/\sigma_{c\ REF}$
	σ_c	Avg (MPa)	
T.S.REF1	2.0	1.90	1.00
T.S.REF2	1.8		
T.S3.120.60.W	2.7	2.65	1.36
T.S4.120.60.W	2.6		
T.S5.120. 60.W.3k	1.7	1.65	0.84
T.S6.120. 60.W.3k	1.6		

596

597 **Table 5. Number of cracks and crack spacing of all tested specimens and theoretical crack spacing.**

Beam	S.L.S				Maximum Load (kN)	U.L.S			EC2	
	No.	Spacing				No.	Spacing (mm)		Spacing (mm)	
		Avg (mm)	Max (mm)	Exp/ Th			Avg	Max	k_1=0.8	k_1=1.6
BM1.REF	5	78	107	1.1	55.8	6	78	107		
BM2.REF	4	93	117	1.1	48.9	5	83	108		
BM3.270.60.a.3k	3	172	175	1.1	40.8	5	88	88	98	163
BM4.270.60.a.3k	4	129	140	0.8	43.4	4	107	128		
BM5.270.60.W.3k	3	126	146	0.9	51.6	4	113	146		

BM6.270.60.W.3k	3	158	187	1.1	40.6	4	113	147
BM7.270.60.W.5k	4	103	117	0.7	43.1	4	103	117
BM8.270.60.W.5k	4	119	158	0.9	48.0	4	119	158

598